Review of Materials Used in TTA-Photon Upconversion Integrated Dye-Sensitized Solar Cells

Berhan Yirci

Received September 28, 2024
Accepted November 25, 2024
Electronic access December 15, 2024

Triplet-triplet annihilation (TTA) has recently gained popularity for its better applicability on solar cells compared to other upconversion mechanisms. Dye-sensitized solar cells are among the most popular solar cells where TTA-UC is applied. Therefore, the choice of material used in the TTA-UC plays a crucial role in the efficiency enhancement of dye-sensitized solar cells, especially by impacting the desired forward and undesired back/decay reactions in the TTA-UC mechanism. This review reviews the effect of material choice on TTA-UC integrated dye-sensitized solar cells. The needed characteristics of materials are determined through short-circuit current density (Jsc) contribution comparisons of different TTA-UC applications on dye-sensitized solar cells. According to this analysis, high Jsc values are acquired in TTA-UC applications that have high triplet-triplet annihilation and energy transfer efficiencies.

Introduction

Photovoltaic solar cells, working by the photoelectric effect, stand as a critical eco-friendly energy source; therefore, increasing their efficiency levels is of great importance to make their use more prevalent. The theoretical efficiency limit of Shockley-Queisser of 34% has been approached significantly in the last 20 years, with silicon cells exceeding 26.8% and thin-film solar cells exceeding 29.1%[1,2,3]. Shockley-Queisser limit occurs due to several reasons, such as the recombination losses of electrons and holes, the thermalization losses of photons that have higher energy than the bandgap, and the transmission losses of photons with lower energy than the bandgap[3]. There have also been efforts to pull the Shockley-Queisser limit by expanding the solar irradiance levels that a solar cell can benefit from. So far, this has been achieved either by photon downconversion or upconversion[4]. Photon upconversion decreases the transmission losses, where the photons with energy lower than the solar cell's bandgap are lost as heat, as seen by the transmission losses portion in Figure 1. It is estimated that by integrating an ideal upconversion mechanism that works with ultimate efficiency, the overall solar cell efficiency can exceed 50% by utilizing sub-bandgap photons[5].

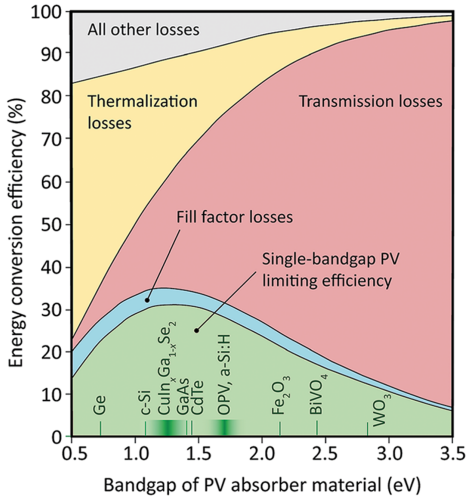

Fig. 1 Illustration of loss mechanisms inside solar cells in percentage concerning the bandgap of the solar cells. This figure is reproduced with Creative Commons permission[6].

In the photon upconversion mechanism, the sequential absorption of pairs of photons leads to a shorter wavelength photon emission, thus utilizing the energies of lower energy photons, as seen in Figure 2. Therefore, the upconversion process is a second harmonic generation, meaning that two photons interacting with a nonlinear material will combine to emit a photon with twice the frequency of absorbed photons[7]. Photon upconversion is achieved through various mechanisms, primarily

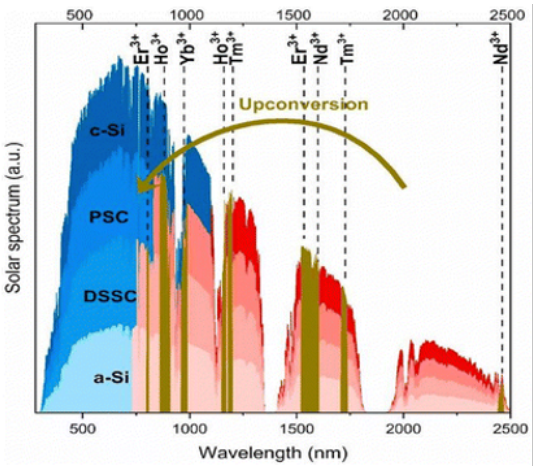

Fig. 2 Graphical illustration of absorbance of different solar cells and the utilization of sub-bandgap photons via upconversion. c-Si: crystalline silicon solar cells; PSC: perovskite solar cells; DSSC: dye-sensitized solar cells; a-Si: amorphous silicon solar cells. This figure is reproduced with Creative Commons permission [12]

by triplet-triplet annihilation (TTA), excited-state absorption (ESA), photon avalanche (PA), and energy transfer upconversion (ETU). However, especially for solar cells, the triplet-triplet annihilation mechanism outperformed others in the visible to near-infrared range due to its capability of working under incoherent light, low flux, and low excitation intensity, which is the case for solar cells under natural sunlight [8,9]. These mainly occur due to the TTA mechanism's long triplet state lifetime and strong singlet-singlet transition oscillator strength, making its transition between singlet and triplet states more efficient [10,11].

Workings Mechanism of Triplet-Triplet Annihilation Upconversion (TTA-UC)

The triplet-triplet annihilation upconversion (TTA-UC) mechanism involves two crucial layers and electronic states. The sensitizer absorbs lower-energy photons and transfers the energy to the emitter layer. The emitter (annihilator) annihilates two low-energy triplets and emits a higher-energy photon. The ground singlet state consists of paired electrons, where the overall spin quantum number equals 0. The triplet state consists of electrons that are not paired, where the overall quantum spin number equals 1.

As depicted in Figure 3(a), the TTA-UC mechanism begins as a low-energy photon ($h\nu_1$) is absorbed by the sensitizer molecule, which excites from its singlet state (S) to its excited singlet state ($^1S^*$). The wavelength of absorption in this case is determined by the emitter molecule's energy difference between its lowest unoccupied molecular orbital (LUMO) and the highest occupied molecular orbital (HOMO), and can be calculated using Planck's equation, $E = \frac{hc}{\lambda}$. Later, the sensitizer undergoes

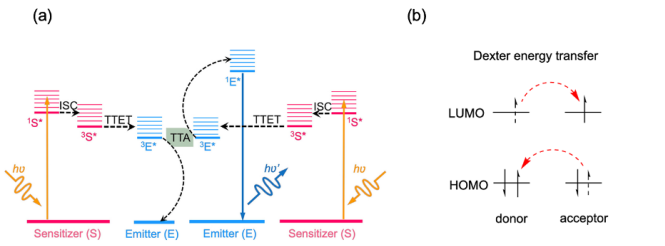

Fig. 3 (a) Representation of triplet-triplet annihilation mechanism. This figure is reproduced with Creative Commons permission [14] (b) Representation of Dexter energy transfer, where LUMO = lowest unoccupied molecular orbital, HOMO = highest occupied molecular orbital. This figure is reproduced with Creative Commons permission [15]

intersystem crossing (ISC) and transitions to its triplet state ($^3S^*$).

Through a Dexter energy transfer mechanism, called triplet-triplet energy transfer (TTET), where an electron exchange occurs between the donor and acceptor molecules, as shown in Figure 3(b), the energy is transferred to the emitter molecule ($^3E^*$). When two triplet-state emitter molecules interact through TTA, one molecule returns to its ground state (E), while the other emitter molecule rises to its excited singlet state ($^1E^*$). Finally, the molecule in its excited singlet state fluoresces and emits a photon ($h\nu_2$), where $\nu_2 > \nu_1$. Thus, by absorbing two low-energy photons, a higher-energy photon is emitted, whose emission wavelength can be calculated according to the energy difference between the molecule's excited singlet state and the ground state. It is a bimolecular reaction since two excited triplet-state molecules are needed for the TTA process. Thus, it brings further necessities, such as higher proximity between molecules, low viscosity, lower mass molecules, and annealing, to increase the efficiency rate. As triplet-triplet energy transfer (TTET) occurs, the emitter's emission wavelength spectrum and the acceptor's absorption spectrum should overlap. Since Dexter energy transfer's rate constant depends on the distance between the emitter and the acceptor logarithmically, the distance becomes the limiting factor [13]. During the TTA-UC mechanism, the Pauli Exclusion Principle is not violated since the electrons in triplet states having the same spin number are located in different orbitals.

Quantum Yields and Limitations of Sub-mechanisms in Triplet-Triplet Annihilation Upconversion

Each subprocess inside the TTA-UC mechanism influences the overall quantum yield in upconversion, which is the ratio between the number of photons emitted/energy output and the number of photons absorbed/energy input. Therefore, the efficiencies of the singlet-singlet transitions, intersystem

crossing, triplet-triplet energy transfer, and triplet-triplet annihilation processes should be enhanced. To have an ideal mechanism for TTA-UC, the ideal paths in Table 1 must be sought while preventing counter paths:

Where

- G: generation rate
- k_2: monomolecular rate constant of $^1S^*$ state decay
- k_{ISC}: intersystem crossing rate constant
- k_3: monomolecular rate constant of 3S* state decay
- k_{TTET}: triplet-triplet energy transfer rate constant
- k_4: monomolecular rate constant of $^3E^*$ state decay
- k_{TTA}: triplet-triplet annihilation rate constant
- $k_{TTA(ss)}$: rate constant of TTA between two sensitizer molecules
- k_1: fluorescence rate constant
- $k_{TTA(se)}$: rate constant of TTA between sensitizer and emitter.
- $^1S^{**}$: second singlet excited state

In Table 1, (A1) corresponds to the absorbance of lower-energy photons by the sensitizer molecule, (A2) to the intersystem crossing, (A3) to the triplet-triplet energy transfer between the sensitizer and emitter molecules, (A4) to the triplet-triplet annihilation between two emitter molecules, and (A5) to the emittance of higher energy photon from the excited singlet state emitter molecule. As the second column corresponds to the decay reactions of the TTA-UC mechanism, the rates in the first column should be maximized while the rates in the second column should be minimized. Furthermore, the energy level difference between $^1S^*$, 3S*, and 3E* should be minimized for the lowest energy loss during intersystem crossing and triplet-triplet energy transfer. 9,16 The energy of 1E* should be slightly lower than twice the energy of 3E* for the maximum energy output. The absorption should be peaking at the desired irradiance levels[9,16]. The second excited tripled state in the emitter should be higher than twice the energy of the first excited triplet state to prevent a loss channel. 9,16 A long triplet lifetime should be possessed[9,16]. These needs make organic dyes, quantum dots (QDs), and perovskite available for sensitizer and polycyclic aromatic hydrocarbon acenes (anthracene, pyrene, perylene, tetracene, rubrene) available for the emitter[17].

The overall upconversion quantum yield is calculated from the equation of $\phi_{UC} = \phi_{ISC}\,\phi_{TTET}\,\phi_{TTA}\,\phi_F$, where ϕ_{ISC} stands for the quantum yield of intersystem crossing, ϕ_{TTET} for the quantum yield of triplet-triplet energy transfer, ϕ_{TTA} for the triplet-triplet annihilation and ϕ_F for the quantum yield of fluorescence[14,16]. The quantum yield of ISC approaches unity in most studies using heavy atoms[18]. Similarly, the quantum yield of fluorescence approaches unity in most emitter materials used in TTA-UC[19]. The ϕ_F may approach unity under conditions such as a high energy gap between the excited singlet state and the triplet state, or a low-temperature environment to reduce the vibrational energy needed to exceed the ISC barrier. Therefore, the main limiting factors of the overall efficiency are the quantum yields of TTA and TTET. To calculate their reaction equations, first, the rate equations of different states should be built according to the reaction paths given in Table 1[9,20,21].

$$\frac{d\left[^1S^*\right]}{dt} = G[S] - k_2\left[^1S^*\right] - k_{ISC}\left[^1S^*\right] \quad (B2)$$

$$\frac{d\left[^3S^*\right]}{dt} = k_{ISC}\left[^1S^*\right] - k_2\left[^3S^*\right] - k_{TTET}\left[^3S^*\right][E] - 2k_{TTA_{(**)}}\left[^3S^*\right]^2$$

$$\frac{d\left[^3E^*\right]}{dt} = k_{TTET}\left[^3S^*\right][E] - k_4\left[^3E^*\right] - 2k_{TTA}\left[^3E^*\right]^2 \quad (B4)$$

$$\frac{d\left[^1E^*\right]}{dt} = 2k_{TTA}\left[^3E^*\right]^2 - k_1\left[^1E^*\right] - k_{TTA_{(*)}}\left[^1S^*\right]\left[^1E^*\right] \quad (B5)$$

$$\frac{d[E]}{dt} = -k_{TTET}\left[^3S^*\right][E] + k_4\left[^3E^*\right] + 2k_{TTA}\left[^3E^*\right]^2 \quad (B6)$$

By assuming the current process as a steady state (d[X]/dt = 0) and dividing the current process rate by the rate of its precursor state rates, the equations of ϕ_{TTA} and ϕ_{TTET} can be found[20].

For ϕ_{TTET}, the current process is denoted by (A3) in Table 1, while the precursor reaction is denoted by (A2).

$$^1\mathrm{S}^* \rightarrow {}^3\mathrm{S}^*, \mathrm{k_{ISC}} \quad (A2)$$

$$^3\mathrm{S}^* + \mathrm{E} \rightarrow \mathrm{S} + {}^3\mathrm{E}^*, \mathrm{k_{TTET}} \quad (A3)$$

Thus,

$$\Phi_{TTET} = \frac{k_{TTET}\left[^3S^*\right][E]}{k_{ISC}\left[^1S^*\right]} \quad (B7)$$

By the steady state assumption of the reaction (A3), it is assumed that d[3S*]/d[t] = 0. Therefore, using the rate equation (B3), the following equality is found:

$$k_{ISC}\left[^1S^*\right] = k_2\left[^3S^*\right] + k_{TTET}\left[^3S^*\right][E] + 2k_{TTA_{(ss)}}\left[^3S^*\right]^2 \quad (C1)$$

By substituting the equation (C1) in the ϕ_{TTET} equation, the following result is found:

$$\Phi_{TTET} = \frac{k_{TTET}\left[3^3S^*\right][E]}{k_2\left[^3S^*\right] + k_{TTET}\left[^3S^*\right][E] + 2k_{TTA_{(ss)}}[3S^*]^2}$$

Table 1. Reaction paths of TTA-UC mechanism.

Ideal TTA-UC Paths		Counter TTA-UC Paths	
S + hν1 → $^1S^*$, G	(A1)	$^1S^*$ → S, k2	(A6)
$^1S^*$ → $^3S^*$, kISC	(A2)	$^3S^*$ → S, k3	(A7)
$^3S^*$ + E → S + $^3E^*$, k_{TTET}	(A3)	$^3E^*$→ E, k4	(A8)
$^3E^*$ + $^3E^*$ → $^1E^*$ + E, k_{TTA}	(A4)	$^3S^*$ + $^3S^*$→ S + $^1S^{**}$, k_{TTA}(ss)	(A9)
$^1E^*$ → E + hν2, k_1 (ν2 > ν1)	(A5)	$^1T^*$ + $^1E^*$ → S + $^1S^{**}$, $k_{TTA(se)}$	(A10)

$$= \frac{k_{TTET}[E]}{k_2 + k_{TTET}[E] + 2k_{TTA_{(ss)}}[3S^*]} \quad (C2)$$

$$\Phi_{TTA} = \frac{k_{TTA}\left[^3E^*\right]^2}{k_{TTET}\left[^3S^*\right][E]} = \frac{k_{TTA}\left[^3E^*\right]^2}{2k_{TTA}\left[^3E^*\right]^2 + k_4\left[^3E^*\right]}$$

$$= \frac{k_{TTA}\left[^3E^*\right]}{2k_{TTA}\left[^3E^*\right] + k_4} \quad (C3)$$

The observations in previously done experiments showed that k2 and k4 dominate other rate constants under low-intensity light[9, 20] . Thus, the TTA-UC system operates quite under its maximum efficiency of 50%. The dominance of the loss channel due to k2 and k4 causes a quadratic excitation power density dependence of upconversion emission until a threshold, where from then on the dependence turns into a linear relationship by the dominance of kTTET and kTTA rate constants over loss channels[22, 23].

Application Types Used in TTA-UC on PV Solar Cells

1. Solid-State

One of the most common application mediums is the solid-state polymer. Inside the glassy polymer matrix, the sensitizer and emitter molecules are annealed[24]. This medium provides a stable structure for solar cell applications, but it has some drawbacks due to heat-related phase separations of the emitter and sensitizer[5, 9] . Furthermore, the medium limits the translational exciton mobility and diffusion. This causes back energy transfer, a loss mechanism, from the emitter to the sensitizer molecules. Thus, the overall TTA-UC efficiency decreases[25, 19] . Even though the structure is initially vulnerable to triplet quenching due to oxygen, the coating can prevent it; yet, practical applications have failed in many attempts[26 27, 28]

2. Rubbery Solid (Elastomeric)

Soft rubbery polymers mostly provide a more efficient medium due to their traits, such as flexibility, high diffusion, and reduced decay rates; however, a threshold temperature should not be exceeded similarly to the solid-state applications to prevent distortion in the matrix's morphology[25, 25]. Rubbery polymers have the advantage of having high transparency, low crystallinity, and low glass transition temperature[5, 21, 25]. Thus, the triplet exciton mobility increases[5]. Yet, choosing the host material according to the chromophore solubility levels is important since otherwise, the required levels of chromophore concentration inside the matrix are not provided to fulfill the exciton mobility and annihilation[25]. Furthermore, the oxygen-caused triplet state quenching mechanism is prevented in rubbery polymers as the chromophores are blended inside the medium[25].

3. Solution-Based (Solvent)

Solution-based TTA applications exceed solid-state and rubbery solid TTA applications, with their superior quantum yields of TTA-UC reaching 30%[9]. However, the solvents used –toluene, benzene, chloroform, acetonitrile, dimethylformamide, and trichloroethane– in these applications are usually toxic, volatile, and flammable, making these applications hazardous and vulnerable to degradation in practical use[9, 17, 29]. Despite these drawbacks, solution-based systems provide higher triplet and singlet mobility, thus increasing the efficiency of the TTA-UC mechanism.

4. Self-Assembled

In self-assembled TTA-UC applications, either physisorption or chemisorption occurs, which means physical or chemical adsorption[30, 31]. This adsorption may occur between the solar cell's semiconductor layer and the TTA-UC emitter/sensitizer or between them. By controlling the positions of TTA-UC molecules, the system doesn't have problems related to phase separation, aggregation, or mobility[31].32 Furthermore, the energy transfer between the sensitizer and emitter may increase due to the reduced distance and energy loss mechanisms[32].

Thin-Film Solar Cells

In addition to their low thickness levels, thin-film solar cells can also be distinguished from other solar cells due to their production techniques, such as sputtering and chemical vapor depositions, which make a low-thickness and flexible structure possible[33]. Although using less material lowers costs, the high degradation rates constrain their commercial use[34]. Dye-sensitized solar cells have a structure where the dye molecules are attached to the electrolyte, which is attached to a counter-electrode catalyst[35]. Thus, the excitation of dyes generates photoelectrons in the dye molecules layer, which then starts redox reactions between the dye molecules-electrolyte and electrolyte-counter electrode[35].The structure of thin-film solar cells may typically be in two forms: substrate or superstate. In

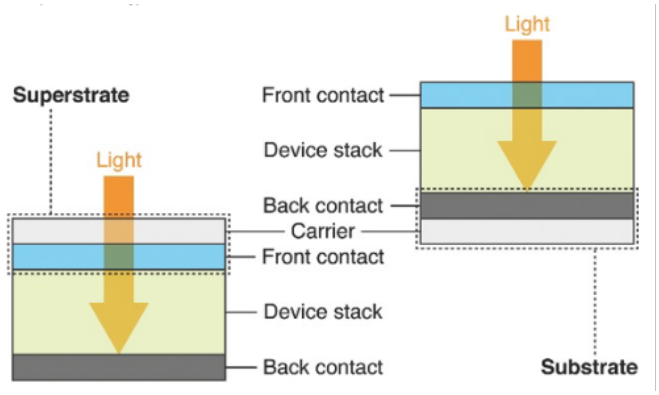

Fig. 4 Superstrate and substrate thin-film solar cell structure illustration. This figure is reproduced with Creative Commons permission [7]

substrate, the deposition occurs on a substrate, such as glass or metal foil, and the substrate acts as an inert layer to support the structure as a backbone [36]. However, in superstrate thin-film solar cells, the substrate glass doesn't just act as a backbone but also as a window channel for illumination, as seen in Figure 4 [33]. Therefore, transparent materials are used in superstrate solar cells [37]. While the order of deposition during production in a superstrate is p-i-n, it is n-i-p in substrate-type thin-film solar cells [38].

Among thin-film solar cells, dye-sensitized solar cells (DSSC) are a remarkable group that is prominent compared to other thin-film solar cells due to their high bandgap values, typically ranging from 1.7 to 2.0 eV [39, 39, 40]. Furthermore, these solar cells are shown to operate well at low-intensity light despite an inferior efficiency at near-infrared with an absorption threshold of approximately 700 nm [9, 41]. Since the upconversion mechanism is applied on sub-bandgap photons, solar cells with high bandgap values like DSSC increase efficiency once the TTA-UC is integrated into the solar cell unit, as seen in Figure 5.

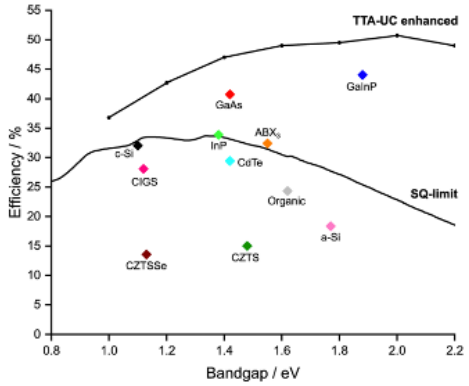

Fig. 5 Graphical representation of efficiency limits of solar cells with and without the TTA-UC applied. Reproduced from Ref. 26 with permission from the Royal Society of Chemistry [29].

Results and Discussion

Materials for TTA-UC in Dye-Sensitized Solar Cells

As each material used inside the TTA-UC affects the quantum yield of the TTA-UC mechanism, it also affects the overall efficiency rate of the solar cell. The following section will compare common materials and techniques used in TTA-UC of dye-sensitized solar cells (DSSC) according to their contribution to the solar cell's current density.

1. Solvent based D149/ benzene/ rubrene/ PQ4PdNA

In their dye-sensitized solar cell integrated TTA-UC study, Andrew Nattestad et al. used the indoline-based dye D149 (C42H35N3O4S3) in their solar cell, which has previously

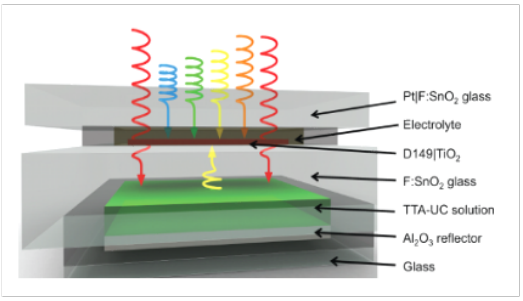

Fig. 6 Andrew Nattestad et al.'s solvent-based TTA-UC integrated DSSC structure; colors represent wavelengths. Reprinted (adapted) with permission from Ref. 43. Copyright 2024 American Chemical Society [42].

shown 9% efficiency in other experiments[42]. For the solvent-based TTA-UC layer, Pd(II) porphyrin-based compound PQ4PdNA for the sensitizer, rubrene (C18H8(C6H5)4) for the emitter, and benzene (C6H6) for the solvent was used as depicted in Figure 6[42]. The absorption of the sensitizer peaks around 670 nm while its phosphorescence peaks at 890 nm, which is an undesired loss mechanism and quenched by the emitter rubrene in this case[42]. Furthermore, rubrene's first excited singlet state is less than twice the energy of its first excited triplet state; however, its second excited triplet state is higher than twice its first excited triplet state, meaning that the product of a TTA causes with high chance an excited singlet state and a ground singlet state[42]. Using benzene as a solvent also provides a higher solubility rate than other solvents, such as toluene, thus decreasing the thickness to around 120 μm[42]. However, using benzene also decreased the device's lifetime by deteriorating the TTA-UC chamber's seal[42]. As a structural problem, the 4 mm gap between the TTA-UC layer and the active layer of DSSC decreased the amount of upconverted light reaching the DSSC active layer[42].

The testing process was implemented using a pump beam and a probe beam[41]. The pump beam is a 670 nm laser diode used to increase the concentration of triplet states in the sensitizer[42]. The probe beam is a low-energy monochromated light source that is insufficient to cause TTA alone[42]. Therefore, the TTA-UC operated when these two beams were directly aligned[42]. When the two beams were unaligned, the upconversion was negligibly low[42]. Thus, by comparing two incident photon to charge carrier conversion efficiency (IPCE) graphs with aligned and unaligned conditions, the effect of TTA-UC was seen[42]. Results under different conditions were compared according to the values of $\Delta J_{sc}/\odot$ (short circuit current density / effective solar concentration)[42]. Thus, the current contribution of the TTA-UC system was analyzed concerning the solar intensity[42].

At 3 $\odot$, a value of $2.25 \times 10^{-3} mA\ cm^{-2}$ was calculated, and the predicted role of TTA-UC in all charge carriers was approximately 1%[42]. The main problem with this system is that the consumption rate of triplets in the emitter is at 5.8%, significantly deteriorating the overall yield[42]. This can be normally solved by increasing the concentration of the emitter/sensitizer and changing the solvent for a higher solubility[42]. However, the triplet decay rate of rubrene is significantly high[42]. Since PQ4PdNA molecules aggregate at high concentrations, the concentration of sensitizer molecules will not solve this problem[42]. As for the sensitizer PQ4PdNA and D149, their Q-band absorption (visible region absorption) at 600-700 nm overlap; thus, the available light intensity decreases for the sensitizer[42]. Therefore, a different material combination with a complementary absorption spectrum should be preferred[42].

2. Self-assembled bilayer/ Zn/ DPPA/ PtTCPP

Both polymer and solvent-based TTA-UC layers in solar cells

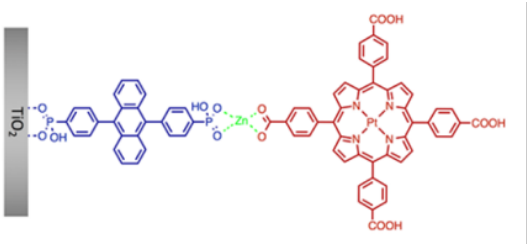

Fig. 7 Sean P. Hill et al.'s self-assembled bilayer TTA-UC integrated DSSC structure. Reprinted (adapted) with permission from Ref. 32. Copyright 2024 American Chemical Society[31]

increase the cost and complexity and cause losses related to diffusion and inner-filtering losses[31]. Aiming to solve these issues, Sean P. Hill et al. used self-assembled bilayers consisting of compounds linked to each other[31]. In their case, the structure respectively consisted of TiO2, DPPA (C12H10N3O3P) for the emitter, Zn, and PtTCPP (C48H28N4O8Pt) for the sensitizer as shown in Figure 7[31]. Since the emitter molecules (DPPA) are directly linked to the TiO2 semiconductor layer, emitter molecules have a high spatial separation and low mobility[31]. Therefore, the system doesn't suffer from aggregation, and the emitter concentration can be high compared to other systems[31]. Thus, it expands the absorption peaks in the emitter molecules' spectrum[31]. Even though the linkage between the emitter and sensitizer increases the rate of triplet-triplet energy transfer from the sensitizers to the emitters, it also incites the Förster resonance energy transfer (FRET), which is a nonradiative loss mechanism in TTA-UC[31]. Thus, the energy transfer from the emitter to the TiO2 decreased[31]. This loss can be minimized by tuning the distance to get the ideal distance or using a different sensitizer/emitter combination to lower the spectral overlap favoring FRET. During analysis, this system achieved a quantum yield of $1.6 \times 10^{-5\%}$ and a Jsc (short-circuit current density) of $0.009 \pm 0.002 mA/cm^2$ under 1 sun illumination[31].

3. Dual emitter solvent based/ D149/ Toluene/ rubrene+BPEA/ PQ4PdNA"

In their study, Rowan W. MacQueen et al. used a system similar to that of Andrew Nattestad's team[42,38]. Their system consisted of dye-sensitized solar cells based on D149 dye, 11 mM rubrene as the emitter, 0.58 mM PQ4PdNA as the sensitizer, and a toluene solvent[43]. To calculate the effect of the TTA-UC layer on the overall efficiency, they benefitted from the pump/probe beam system[43]. In the end, they had a TTA quantum yield (ϕ_{TTA}) of 1.09%[43]. Due to rubrene's slow TTA rate and the high decay rate of triplets, researchers Yuen Yap Cheng et al. determined to solve this issue by integrating a second emitter molecule to create a dual-emitter TTA-UC system[44]. In this trimolecular composition, they similarly used a D149-based DSSC, toluene solvent, and differently 2mM rubrene, 5.1 mM BPEA as the emitters, and 0.8 mM PQ4PdNA as the sensitizer[44]. Thus, they were able to increase the efficiency

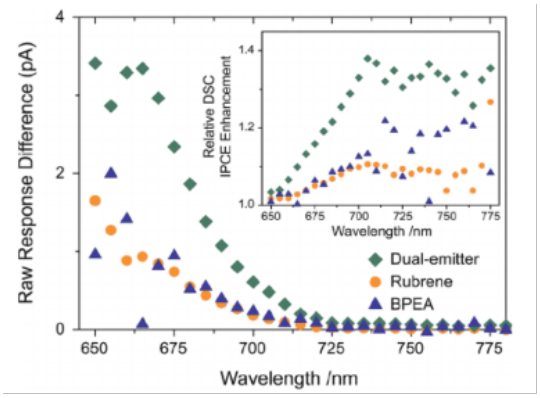

Fig. 8 In Yuen Yap Cheng et al.'s study, the incident photon enhanced current efficiency under different emitters. Reproduced from Ref. 46 with permission from the Royal Society of Chemistry[44].

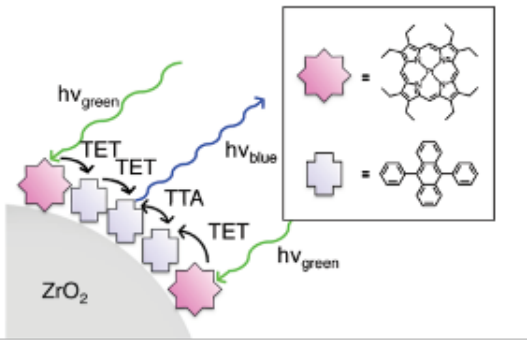

Fig. 9 Jonas Sandby Lissau et al.'s DPA emitter-based former TTA-UC structure. Reprinted (adapted) with permission from Ref. 31. Copyright 2024 American Chemical Society[45]

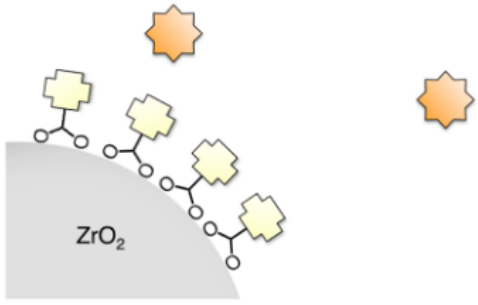

Fig. 10 Jonas Sandby Lissau et al.'s MTAB emitter-based latter TTA-UC structure; anchored emitters denoted by the cross; sensitizers denoted by the star. Reprinted (adapted) with permission from Ref. 30. Copyright 2024 American Chemical Society[30]

of the systems since the rate of self-[44] absorption and self-quenching of the emitter decreased[44]. It is determined that while BPEA increased the efficiency of the TTA process, the emission was still mainly done by rubrene molecules; thus, BPEA acted more as an energy transfer bridge between the TTA process and the emission from rubrene[44]. With this system, they were able to get approximately a Jsc of 4.5 - 5 x 10-3 mA cm-2 at 3 ⊙, and an incident photon to current efficiency (IPCE) enhancement due to the presence of TTA-UC layer was calculated as 1.4% at 700-775 nm, as seen in Figure 8[44].

4. Physisorbed in solvent/ Water/ DPA/ PtOEP vs. Chemisorbed in solvent/ BuN/ MTAB/ PtOEP

Jonas Sandby Lissau et al. aimed to utilize TTA-UC in DSSC by adsorbing emitter molecules to the semiconductor[45]. They used DPA emitter dye molecules (9,10-diphenyl anthracene) and PtOEP sensitizer dye molecules (platinum(II) octaethylporphyrin) physisorbed (physically adsorbed) to ZiO2, as seen in Figure 9[45]. However, this system suffered from PtOEP aggregation, keeping the excitation energy and limiting mainly the TTET process[45]. Also, the presence of oxygen molecules caused the quenching of triplet states[45]. Furthermore, the use of polar solvent water and nonpolar emitter DPA was thought to limit the TTA by causing problems in orientation[45]. The orientation problems prevented the needed orbital overlapping for the Dexter energy transfer, lowering efficiency[45].

Jonas Lissau and his coworkers replaced DPA with MTAB (methyl 4-(10-p-tolylanthracen-9- yl)benzoate) to solve these issues through several chemical reactions[30]. These sensitizer molecules were later chemisorbed (chemically adsorbed) to the ZiO2 layer as depicted in Figure 10[30]. Since the anchoring process was done by chemisorption, the use of heat wouldn't cause the desorption (release from adsorption) of sensitizers from the TiO2 semiconductor layer[30]. Thus, the system was sealed with an argon atmosphere, which required a heat-intensive process[30]. By using butyronitrile (BuN) solvent, which shows good performance with electrolytes and less polarity compared to water, the TTET efficiency among emitters and unaggregated mobility of PtOEP increased due to better orientation[30]. Through spectroscopy and estimations, it is found that while the water and DPA-based former study showed an ϕ_{UC} of 0.0006%, the later study with MTAB and BuN showed an ϕ_{UC} of 0.04 %[30]. However, the system suffers from a limited energy transfer process from the sensitizers to the emitters[30]. This problem could be solved by increasing the concentrations of sensitizer/emitter molecules or anchoring sensitizer molecules through a metal atom or organic compound[30]. Thus, the energy transfer would have a higher reaction rate[30]. This system was not integrated into the solar cell during analysis, but it still gives valuable insights for applying TTA-UC in DSSC.

5. Self-assembled bilayer/ Zn/ A/ PdP vs. Trilayer/ Zn/ A/ PdP/ PtP

In their study, Tristan Dilbeck et al. implemented TTA-UC on DSSC by self-assembled trilayers[32]. Through soaking processes, the TiO2 semiconductor surface was first bound by 4,4'-(anthracene-9,10-dial)bis(4,1-phenylene) diphosphonic acid (A) that acts as the emitter, and then respectively the sensitizer layers of PdP (Pd(II) meso-tetra(4- carboxyphenyl)porphine) and

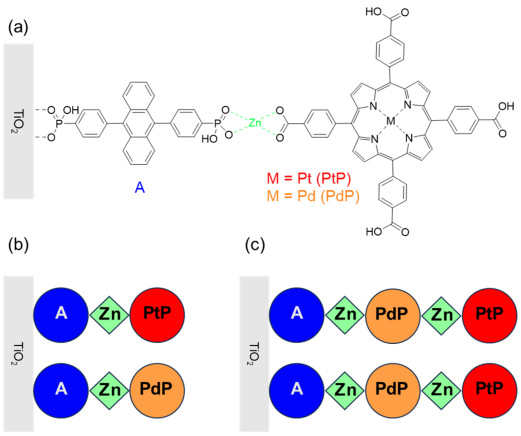

Fig. 11 (a) Molecular structure of self-assembled bilayer TTA-UC. (b) Bilayer TTA-UC system. (c) Trilayer TTA-UC system.

PtP (Pt(II) meso-tetra(4- carboxyphenyl)porphine) were linked through Zn molecules as depicted in Figure 11(c)[32]. As PdP and PtP sensitizers came together with absorptions respectively at 510-550 nm and 490-530 nm, the absorbance spectrum of the TTA-UC layer increased overall[32]. Furthermore, a high sensitizer concentration was achieved[32]. Inside the system, Co3+ was chosen as the redox mediator since its absorbance at the visible spectrum is low, thus not causing absorption loss[32]. The trilayer system showed an efficiency of 0.0012%, two orders of magnitude higher than the bilayer system, which lacked PdP molecules, as depicted in Figure 11(a) and (b)[32]. This system also increased the distance between the semiconductor TiO2 and redox mediator Co3+, which decreased the recombination rate[32]. In the incident photon to current efficiency (IPCE) graph, it was seen that the trilayer TTA-UC system peaked at 515 nm with 1.28%[32]. The Jsc was 7.41 x 10-2 mA cm-2 under 1 ⊙[32]. Yet, for higher efficiency, the energy transfer efficiency among A-PdP-PtP should be increased with possibly a different metallic element linkage; back energy transfer from acceptor to sensitizer should be minimized; the complementary absorption spectrum of sensitizers should be optimized either with tuning or a different material choice; yield of injection from the emitter to the semiconductor should be maximized; and lastly, the triplet quenching mechanism rates should be minimized possibly with an inert gas atmosphere seal.

6. Adsorbed/ Alkyl chain spacer/ ADDA/ PtTPO

In their study, Tatsuro Morifuji et al. implemented TTA-UC on a DSSC by adsorbing emitter Pt(II)-8-[4-(10,15,20-triphenylporphyrin -5-yl) benzamido] - octanoic acid dye (PtTPO) to the mesoporous TiO2 semiconductor with an alkyl chain spacer through a day-long soaking in the solution[46]. Later on, the same procedure was applied to the sensitizer 4′ - (anthracene-9,10-diyl) dibenzoic acid (ADDA) as depicted in Figure 12[46]. The concentration of the emitter ADDA and sensitizer PtTPO was respectively

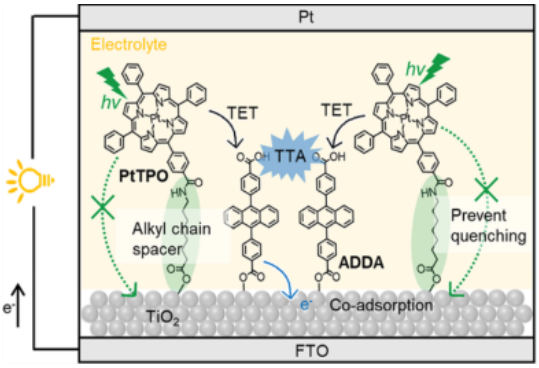

Fig. 12 Tatsuro Morifuji et al.'s structure of ADDA/PtTPO adsorbed TTA-UC. This figure is reproduced with Creative Commons permission[46].

1 mM and 0.1 mM[46]. Due to using an alkyl chain spacer, the distance between the semiconductor and the sensitizer increased[46]. As a result, the rate of triplet sensitizer quenching due to unwanted energy transfer from the sensitizer to the semiconductor decreased since the distance between them increased[46]. As a result, the efficiency of the solar cell was 0.72%, and under 1 sun, the photocurrent contribution of the TTA-UC unit was 0.036 mA cm^{-2}[46]. However, the decay of emitter triplet states limited the system's efficiency due to low orbital overlap with other emitter triplet states[46]. To solve this problem, a different emitter material or a higher concentration of ADDA should be used[46].

Comprehensive Comparison and Future Prospects of TTA-UC in DSSC

The TTA-UC applications on DSSC can be compared by the metric determined as the short circuit current density (Jsc) concerning the solar intensity (⊙), as shown in Table 2. The higher the Jsc is, the higher the current contribution of the TTA-UC means. Among the prominent applications of TTA-UC on DSSC, it is seen that the most efficient ones (4.275x10-2, 7.41x10-2, 3.6x10-2) are the applications where the drawbacks due to triplet-triplet energy transfer (TTET) and the efficiency of triplet-triplet annihilation (TTA) is alleviated by the use of different structures (alkyl spacer, adsorption) or dual materials. Yet, in most of the studies done so far, it has been seen that the main problem with the overall TTA-UC quantum yield stems from the efficiency of TTA and energy transfer.

The problems regarding the energy transfer from the sensitizer to the emitter were eased either by using less polar solvents or by anchoring these molecules either among themselves or on the semiconductor layers, such as TiO_2 and ZiO_2. The adsorption technique further prevented aggregation and phase separation problems. However, in some cases, these attempts further increased the rate of some loss mechanisms, primarily

Table 2. TTA-UC Jsc and ⊙ values in DSSC.

TTA-UC Application Name	Short Circuit Current Density Jsc (mA cm-2)	Solar Intensity ⊙ (1000W/m2)	Ref.
Solvent-based D149/ benzene/ rubrene/ PQ4PdNA	2.25×10^{-3}	3	43
Self-assembled bilayer TiO2 / Zn/ DPPA/ PtTCPP	$9 \pm 2 \times 10^{-3}$	1	32
Dual-emitter solvent based D149/ Toluene/ rubrene+BPEA/ PQ4PdNA	$4.275 \pm 0.225 \times 10^{-2}$	3	47
Self-assembled trilayers TiO2/ Zn/ PdP+PtP/ A	7.41×10^{-2}		33
Anchored with an alkyl spacer TiO2/ alkyl spacer/ ADDA/ PtTPO	3.6×10^{-2}	1 1	47

the back energy transfer from the emitter to the sensitizer. Thus, the energy gathered from low-energy photons wasn't effectively used to create emitter-excited singlet states. As for the efficiency of the TTA process, there have been problems related to the emitter molecules' high triplet decay rates, which limit the concentration of emitter triplet states. These problems were reduced mainly by integrating a second emitter molecule into the TTA-UC system. However, the emitter and dyes should be chosen carefully so that their absorbance spectrum will not overlap with the sensitizer's to exploit a wider energy range of photons. Yet, the efficiency of TTA-UC systems in dye-sensitized solar cells is still not high enough for commercial use. To overcome this issue, new material combinations should be explored. The following steps may form these combinations:

I. Efficiently integrating multiple emitter molecules to benefit from specific reaction paths of each emitter

II. Anchoring these emitter molecules to the solar cell's semiconductor layer through chemisorption or choosing a solvent that will make TTA-UC molecules highly soluble

III. Choosing a sensitizer molecule whose absorption spectrum will not overlap with the other molecules

IV. Efficiently integrating multiple sensitizer molecules to broaden the absorption spectrum

V. Tuning energy levels or choosing the emitter and sensitizer molecules so that the energy levels of the emitter and sensitizer's singlet and triplet states prevent energy losses during state transitions and energy transfers

VI. Sealing the system with an inert gas to prevent oxygen-based quenching Only after implementing these steps can a dye-sensitized solar cell efficiency enhancement from 30% to 40% be achieved[45].

Conclusion

To achieve commercial use, a triplet-triplet annihilation upconversion system is key in dye-sensitized solar cells. Despite promising high-efficiency rates in the future, TTA-UC systems in DSSC still suffer from energy loss and degradation mechanisms. In this review, it's been seen that even though commercialization is not possible with TTA-UC applications, material choice plays a crucial role in the efficiency of TTA-UC systems. TTA-UC systems with dual emitters, anchoring structures, and self-assembled layers currently possess a higher chance for commercial applicability in the future. For future studies, to achieve a stable and highly efficient TTA-UC integrated into dye-sensitized solar cells, particular importance should be given to exploring new material combinations that will achieve the highest yield according to the desired forward and undesired back/decay/quenching reactions in the TTA-UC mechanism. With a highly efficient TTA-UC layer that can be integrated, dye-sensitized solar cells may replace silicon-based solar cells' dominance over the market, thanks to their higher efficiency limit that will be possessed through TTA-UC applications. Thus, acquiring a high-efficiency dye-sensitized PV solar cell technology may make a low-carbon and efficient energy generation system prevalent in the energy market

Acknowledgments

I want to thank my mentor, Avery Baumann, for her help and valuable feedback during my study.

References

1 LONGi, *At 26.81%, LONGi Sets a New World Record Efficiency for Silicon Solar Cells*, https://www.longi.com/en/news/propelling-the-transformation/, Accessed: 2024-09-01.

2 S. E. Ltd., *Alta Sets Flexible Solar Record with 29.1% GaAs Cell*, https://optics.org/news/9/12/19, Accessed: 2024-09-01.

3 W. Shockley and H. J. Queisser, *J. Appl. Phys.*, 1961, **32**, 510–519.

4 D. Verma, T. O. Saetre and O.-M. Midtgard, 2012 38th IEEE Photovoltaic Specialists Conference, 2012.

5 B. Joarder, N. Yanai and N. Kimizuka, *J. Phys. Chem. Lett.*, 2018, **9**, 4613–4624.

6 J. Pedrini and A. Monguzzi, *J. Photonics Energy*, 2017, **8**, 1.

7 M. Hösel, D. Angmo, R. R. Søndergaard, G. A. dos Reis Benatto, J. E. Carlé, M. Jørgensen and F. C. Krebs, *Adv. Sci. (Weinh.)*, 2014, **1**, year.

8 D. Lin, J. Zhong, S. Ji, Z. Yuan, L. Xing, Q. He, H. Zhang and Y. Huo, *Dyes Pigm.*, 2021, **185**, 108912.

9 T. F. Schulze and T. W. Schmidt, *Energy Environ. Sci.*, 2015, **8**, 103–125.

10 X. Cao, B. Hu and P. Zhang, *J. Phys. Chem. Lett.*, 2013, **4**, 2334–2338.

11 J. Zhao, S. Ji and H. Guo, *RSC Adv.*, 2011, **1**, 937.

12 A. Ghazy, M. Safdar, M. Lastusaari, H. Savin and M. Karppinen, *Sol. Energy Mater. Sol. Cells*, 2021, **230**, 111234.

13 *Dexter energy transfer*, *Chemistry LibreTexts*, https://chem.libretexts.org/Bookshelves/Physical_and_Theoretical_Chemistry_Textbook_Maps/Supplemental_Modules_(Physical_and_Theoretical_Chemistry)/Fundamentals/Dexter_Energy_Transfer, Accessed: 2024-09-01.

14 B. Zhang, K. D. Richards, B. E. Jones, A. R. Collins, R. Sanders, S. R. Needham, P. Qian, A. Mahadevegowda, C. Ducati, S. W. Botchway and R. C. Evans, *Angew. Chem. Int. Ed Engl.*, 2023, **62**, year.

15 C. G. Thomson, A.-L. Lee and F. Vilela, *Beilstein J. Org. Chem.*, 2020, **16**, 1495–1549.

16 Y. Y. Cheng, T. Khoury, R. G. C. R. Clady, M. J. Y. Tayebjee, N. J. Ekins-Daukes, M. J. Crossley and T. W. Schmidt, *Phys. Chem. Chem. Phys.*, 2010, **12**, 66–71.

17 C. Gao, W. W. H. Wong, Z. Qin, S.-C. Lo, E. B. Namdas, H. Dong and W. Hu, *Adv. Mater.*, 2021, **33**, year.

18 M. P. Rauch and R. R. Knowles, *Chimia (Aarau)*, 2018, **72**, 501.

19 A. Kalpattu, T. Dilbeck, K. Hanson and J. T. Fourkas, *Phys. Chem. Chem. Phys.*, 2022, **24**, 28174–28190.

20 V. Gray, D. Dzebo, M. Abrahamsson, B. Albinsson and K. Moth-Poulsen, *Phys. Chem. Chem. Phys.*, 2014, **16**, 10345–10352.

21 T. N. Singh-Rachford and F. N. Castellano, *Coord. Chem. Rev.*, 2010, **254**, 2560–2573.

22 A. Monguzzi, J. Mezyk, F. Scotognella, R. Tubino and F. Meinardi, *Phys. Rev. B Condens. Matter Mater. Phys.*, 2008, **78**, year.

23 A. Haefele, J. Blumhoff, R. S. Khnayzer and F. N. Castellano, *J. Phys. Chem. Lett.*, 2012, **3**, 299–303.

24 J. Duan, Y. Liu, Y. Zhang, Z. Chen, X. Xu, L. Ye, Z. Wang, Y. Yang, D. Zhang and H. Zhu, *Sci. Adv.*, 2022, **8**, year.

25 Y. C. Simon and C. Weder, *J. Mater. Chem.*, 2012, **22**, 20817.

26 J.-H. Kim, F. Deng, F. N. Castellano and J.-H. Kim, *ACS Photonics*, 2014, **1**, 382–388.

27 O. S. Kwon, J.-H. Kim, J. K. Cho and J.-H. Kim, *ACS Appl. Mater. Interfaces*, 2015, **7**, 318–325.

28 C. Wohnhaas, A. Turshatov, V. Mailänder, S. Lorenz, S. Baluschev, T. Miteva and K. Landfester, *Macromol. Biosci.*, 2011, **11**, 772–778.

29 A. J. Carrod, V. Gray and K. Börjesson, *Energy Environ. Sci.*, 2022, **15**, 4982–5016.

30 J. S. Lissau, D. Nauroozi, M.-P. Santoni, S. Ott, J. M. Gardner and A. Morandeira, *J. Phys. Chem. C Nanomater. Interfaces*, 2013, **117**, 14493–14501.

31 S. P. Hill, T. Dilbeck, E. Baduell and K. Hanson, *ACS Energy Lett.*, 2016, **1**, 3–8.

32 J. S. Lissau, J. M. Gardner and A. Morandeira, *J. Phys. Chem. C Nanomater. Interfaces*, 2011, **115**, 23226–23232.

33 K. L. Chopra, P. D. Paulson and V. Dutta, *Prog. Photovolt.*, 2004, **12**, 69–92.

34 E. T. Efaz, M. M. Rhaman, S. A. Imam, K. L. Bashar, F. Kabir, M. D. E. Mourtaza, S. N. Sakib and F. A. A. Mozahid, *Eng. Res. Express*, 2021, **3**, 032001.

35 X. Deng and E. A. Schiff, *Handbook of Photovoltaic Science and Engineering*, Wiley, 2003, pp. 505–565.

36 A. Adeyinka, O. Mbelu, D. Yahya and Y. Adediji, *World Academy of Science, Engineering and Technology*, 2023, **17**, year.

37 S. T. Yussuf, K. C. Nwambaekwe, M. E. Ramoroka and E. I. Iwuoha, *Materials Today Sustainability*, 2023, **21**, 100287.

38 *McEvoy's Handbook of Photovoltaics*, Elsevier, 2018.

39 C. R. Holkar, S. S. Jain, A. J. Jadhav and D. V. Pinjari, *Nanomaterials for Green Energy*, Elsevier, 2018, pp. 433–455.

40 R. W. Miles, K. M. Hynes and I. Forbes, *Prog. Cryst. Growth Charact. Mater.*, 2005, **51**, 1–42.

41 A. Nattestad, Y. Y. Cheng, R. W. MacQueen, G. G. Wallace and T. W. Schmidt, *J. Vis. Exp.*, 2014.

42 A. Nattestad, Y. Y. Cheng, R. W. MacQueen, T. F. Schulze, F. W. Thompson, A. J. Mozer, B. Fückel, T. Khoury, M. J. Crossley, K. Lips, G. G. Wallace and T. W. Schmidt, *J. Phys. Chem. Lett.*, 2013, **4**, 2073–2078.

43 R. W. MacQueen, Y. Y. Cheng, A. N. Danos, K. Lips and T. W. Schmidt, *RSC Adv.*, 2014, **4**, 52749–52756.

44 Y. Y. Cheng, A. Nattestad, T. F. Schulze, R. W. MacQueen, B. Fückel, K. Lips, G. G. Wallace, T. Khoury, M. J. Crossley and T. W. Schmidt, *Chem. Sci.*, 2016, **7**, 559–568.

45 T. Dilbeck, S. P. Hill and K. Hanson, *J. Mater. Chem. A Mater. Energy Sustain.*, 2017, **5**, 11652–11660.

46 T. Morifuji, Y. Takekuma and M. Nagata, *ACS Omega*, 2019, **4**, 11271–11275.